A Nature Portfolio journal



https://doi.org/10.1038/s43247-025-02845-6

Less water from glaciers during future megadroughts in the Southern Andes

Check for updates

Álvaro Ayala ® ^{1,2} , Eduardo Muñoz-Castro ® ^{3,4,5,6}, Daniel Farinotti ® ^{7,8}, David Farías-Barahona ® ⁹, Pablo A. Mendoza ® ^{3,10}, Shelley MacDonell ® ^{1,11}, James McPhee ® ^{3,10}, Ximena Vargas ® ³ & Francesca Pellicciotti ® ^{2,12}

Glacier melt sustains water discharge from mountain basins during droughts, but ongoing glacier retreat threatens this fundamental capacity. Here, we assess the response of glaciers in the Southern Andes to one of the most severe, persistent, and extensive droughts on record in South America (2010-present), and to projected end-of-century megadroughts. Using glacio-hydrological numerical simulations, we show that despite a mean annual precipitation deficit of 36%, glacier runoff in 2010-2019 remained almost unaltered compared to the preceding decade (2000-2009), sustained by a 10% loss of total ice volume. However, simulations of future glacier evolution indicate that annual and summer glacier runoff could decline by up to $20 \pm 11\%$ and $48 \pm 6\%$, respectively, during end-of-century megadroughts compared to pre-2010 levels. Our results project a weakening of the glacier's buffering role against precipitation deficits during extreme droughts, increasing water scarcity for ecosystems and livelihoods in the mountain regions of South America.

Meteorological droughts can lead to water-stressed ecosystems^{1,2} and produce dramatic impacts for human societies, including reduced public water supply, crop failures and energy shortages³⁻⁵. The term megadrought has been used to describe persistent multi-year precipitation deficits that result in severe hydrological, ecological, agricultural or socioeconomic droughts⁶⁷. Over the past two decades, severe droughts in California⁸, Europe⁹, and China¹⁰ have caused large economic losses and damage to ecosystems. Because climate models project an increase in both the frequency and intensity of droughts 11,12, serious concerns have emerged about the effect of future droughts and their impacts on societies^{11,13}. A notorious drought of recent decades has been the Chilean megadrought¹⁴, which has affected the central regions of Chile and western Argentina since 2010 (Fig. 1a,b) causing severe hydrological and societal impacts. With a population over twenty million people and a strong dependence on meltwater from the Andes Cordillera¹⁵, central Chile and western Argentina have based a large part of their economies on industries that are greatly affected by water scarcity, such as agriculture and mining^{16–18}. The Chilean megadrought stands out in the instrumental¹⁹ and paleoclimatic record in South America^{20,21} due to its persistence (from 2010 to present), severity and large spatial extent, spanning from approximately 30 to 40°S and from coastal Chile to the eastern slopes of the Andes (Fig. 1a, b and Supplementary Fig. 1). Annual precipitation deficits during the megadrought have ranged between 25% and 45%^{14,19}. The Chilean megadrought ranks in the top twenty worldwide in the period 1987–2016 in terms of duration and severity^{22,23}. The major causes of the Chilean megadrought lie in a persistent large-scale circulation pattern that blocks the passage of extratropical storms over central Chile (Supplementary Note 1). This configuration has been likely driven by a negative phase of the Pacific Decadal Oscillation (PDO) (associated to natural variability) and a positive phase of the Southern Annular Mode (SAM) (associated with anthropogenic forcing)^{19,24}. The Chilean megadrought has had cascading effects on streamflow²⁵, lake levels²⁶, soil moisture²⁷, wildfires²⁸, sediment export²⁹, and glacier mass balance³⁰. The combination of these effects can be particularly critical in arid and semi-arid mountain regions where water shortages can trigger social conflicts^{31,32}.

The impact of the Chilean megadrought on the cryosphere of the Southern Andes provides a unique opportunity to understand the role of glaciers in buffering sustained precipitation deficits. The Southern Andes extends from 20 to 55°S and contains more than 15,000 glaciers³³. While

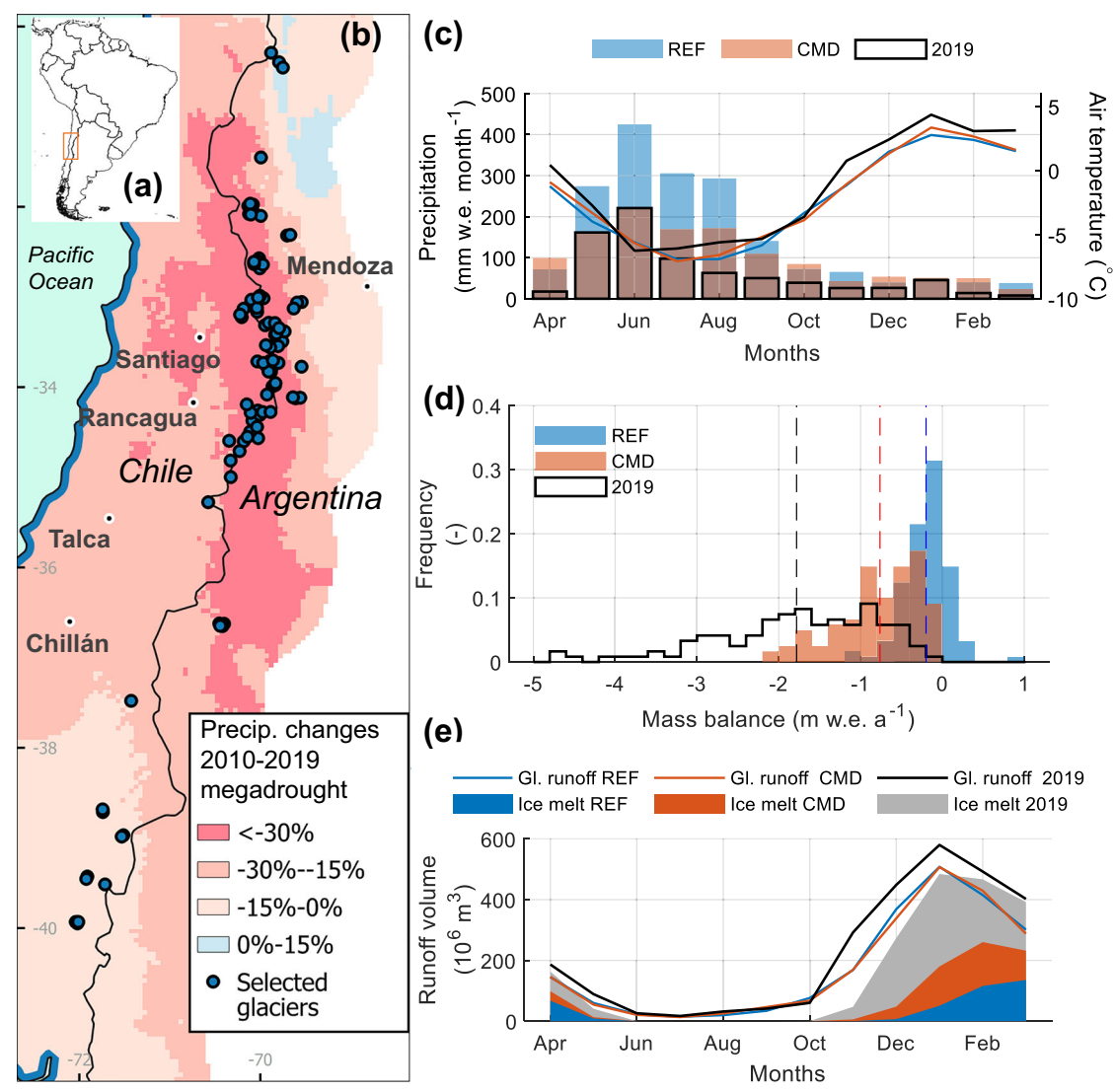


Fig. 1 | Hydrological response of glaciers to the Chilean megadrought (2010–2019, CMD) compared to the reference period (2000–2009, REF).

a Location of the study domain in South America. b Location of the 100 largest glaciers in the RGIv6.0 between 30°S and 40°S, along with relative precipitation changes in the CMD. White colour over Argentina represents areas where the CR2Met precipitation product is not available ("no data"). c Mean monthly precipitation totals and mean air temperature for the selected glaciers (downscaled and

bias-corrected forcing data for TOPKAPI-ETH). "2019" stands for the extremely dry year of 2019. **d** Histograms of annual mean glacier mass balance (TOPKAPI-ETH outputs), the distributions were tested to be different at a 5% significance level. Dashed vertical lines show the mean of each distribution (**e**) Monthly glacier runoff (lines) and ice melt (shaded areas) total volume for REF, CMD and 2019 (TOPKAPI-ETH outputs).

seasonal snowmelt is the main source of runoff for areas adjacent to the Andes^{34,35}, glacier meltwater compensates for the lack of other freshwater sources during dry periods. For example, in recent decades, glacier runoff has contributed approximately 15% to the annual discharge of rivers in Central Chile (e.g. the upper Maipo and Aconcagua catchments), with contributions exceeding 50% during summer, depending on the elevation of the river outlet 30,36,37. Around the world, glacier meltwater has been able to compensate for precipitation deficits during droughts^{32,38}, but this buffering capacity is threatened by glacier retreat^{39,40}. Although accelerated glacier melt in glacierised basins can lead to a transient increase in annual runoff (known as "peak water"), meltwater discharge is expected to decrease if glacier retreat persists 42. This has been observed in the Southern Andes across central Chile and Argentina, where runoff from glaciers has decreased compared to 20th century reconstructions due to glacier mass loss^{38,43,44}. Previous work suggests that the glaciers of the Southern Andes have played a key role in sustaining water systems during the ongoing megadrought, but their capacity to buffer precipitation deficits during future droughts will be threatened by their expected continued retreat in the 21st

century⁴¹. The relatively low level of large-scale human intervention in the Southern Andes (compared to, for example, the European Alps) enables the analysis of a natural system and provides an opportunity to analyse the impacts of future multi-year droughts on mountain water resources.

Here, we examine the hydrological response of glaciers during a 10-year sub-period of the Chilean megadrought (2010-2019) and during megadroughts projected to occur by the end of the century under global climate projections. We use the TOPKAPI-ETH glacio-hydrological model^{37,45} to simulate the evolution, mass balance and runoff of the 100 largest glaciers in the Southern Andes between 30°S and 40°S, which is the latitudinal range most affected by the Chilean megadrought. The selected 100 glaciers comprise a total of 82 km³ of ice volume, representing 65.8% of the total glacier volume in the region (Supplementary Fig. 1). Their outlines are extracted from the Randolph Glacier Inventory v6.0 (RGIv6.0)³³. TOPKAPI-ETH is a spatially distributed physics-based model that explicitly parameterises the main processes governing glacierized environments, including mass redistribution due to ice flow, avalanching and ice melt under debris (Methods). The model considers snow albedo decay and

distributed ice albedo, which are key elements to understand the impact of snowfall reduction on surface melt^{46,47}, as well as geometry changes due to glacier dynamics⁴⁸, which are essential in century-scale simulations⁴⁹. We run the model at high horizontal (100 m) and temporal (3-hour) resolutions. We calibrate and evaluate the model parameters for each selected glacier using a global geodetic glacier mass balance dataset⁴⁴ and satellitederived albedo retrievals from MODIS⁵⁰ (Supplementary Figs. 2-7). Simulations are forced with meteorological gridded data for hydrological years (1 April to 31 March) during the period 2000-2019 extracted from CR2Met v2.0⁵¹ and ERA5 reanalysis⁵². The model is then used to generate projections for the period 2000-2099 using outputs from four Global Climate Models (GCM) and two Representative Concentration Pathways (RCP) taken from the fifth phase of the Climate Model Intercomparison Project (CMIP5)⁵³: a moderate (RCP2.6) and a high (RCP8.5) future greenhouse gas (GHG) emission scenario. We downscale and biascorrect the coarse-resolution outputs of the GCMs to adjust the spatial mismatches and systematic biases when compared to the glacier scale^{54,55} (Supplementary Figs. 8-9). We use 2000-2009 as a reference period for subsequent comparisons of glacier runoff and other variables, since it has been identified as a period of near-neutral glacier mass balance in the study area^{56,57}. End-of-century megadroughts are assumed to correspond to the 10-year period with the lowest precipitation that occurs during 2075–2100 for each combination of GCM and RCP (Methods and Supplementary Fig. 10). Based on previous studies, we define glacier runoff as the sum of meltwater from glacier ice and seasonal snow plus liquid precipitation within the glacier area at the start of the simulations (i.e. year 2000)⁴¹. TOPKAPI-ETH explicitly differentiates these runoff components, which are used to analyse internal shifts in the glacier hydrology. Changes in glacier runoff are evaluated on an annual and summer (JFM) basis.

Results

Glacier response to the Chilean megadrought

The Chilean megadrought has been defined by a strong and persistent reduction in precipitation across Chile and western Argentina compared to the preceding 30 years (Supplementary Fig. 11). Hereafter, we refer to changes compared to annual averages in the 2000-2009 reference period, unless otherwise stated. Glacier area and volume changes are computed with respect to the initial values of the simulations (year 2000). Precipitation reductions in 2010-2019 ranged from less than 15% in areas south of 37°S to more than 30% between 31°S and 37°S, where most of the glaciers are located (Fig. 1b and Table 1). Precipitation over the selected glaciers changed by $-36 \pm 12\%$ (average and standard deviation from the sample of glaciers), with most of this decrease concentrated in the austral winter (JJA), when the bulk of precipitation occurs (Fig. 1c, left axis). Compared to precipitation, changes in air temperature were less pronounced, with a warming of 0.2 ± 0.1 °C (Fig. 1c, right axis). TOPKAPI-ETH results show that the frequency distribution of glacier mass balance became increasingly skewed towards negative values during the megadrought, with the average glacier mass balance becoming four times more negative (-0.8 ± 0.5 m w.e. a⁻¹ compared to -0.2 ± 0.3 m w.e. a⁻¹ in the 2000–2009 period, Fig. 1d), leading to a 10% loss of the total ice volume existing at the start of the megadrought. Total glacier runoff volume from the 100 selected glaciers decreased only slightly during the megadrought (decrease of 1%), with most glaciers (95%) experiencing glacier runoff changes between -20 and +20% (Supplementary Fig. 12). Ice melt, however, increased by 118% during the megadrought, offsetting the decrease in snowmelt (32%) associated with precipitation decline (Fig. 1c and Table 1). We estimate that the selected glaciers provided an additional ice melt contribution of 454 · 10⁶ m³ a⁻¹ during the megadrought, which is equivalent to twice the capacity of El Yeso, the largest reservoir for the drinking water supply of Santiago, Chile⁵⁸. The changes observed during the megadrought were amplified in the extremely dry and warm year of 2019 (Fig. 1c-e), one of the driest years on record⁵⁹ and the warmest year within the megadrought period in our study domain. Precipitation in 2019 was $66 \pm 23\%$ lower than in the reference period (Fig. 1c), while air temperature increased by 0.9 ± 0.2 °C (Fig. 1c) and the average glacier mass balance was -1.8 ± 1.0 m w.e. a^{-1} (Fig. 1d). Glacier runoff and ice melt were 25% and 390% higher, respectively, compared to the reference period (Fig. 1e).

Climate projections and future glacier evolution

Climate projections indicate an increase in air temperature, leading to a massive loss of glacier volume. Air temperature anomalies over the selected glaciers are similar for both RCPs in 2000-2020 (Fig. 2a), after which they begin to diverge considerably, with strong differences emerging from 2040 onwards. By the end of the century, mean annual temperatures in the 2090-2099 decade are projected to increase by 1.5 ± 0.3 °C (average and standard deviation over GCMs) under RCP2.6 and 4.7 ± 0.4 °C, under RCP8.5. Differences in projected annual precipitation changes between the scenarios are less pronounced (Fig. 2b). Annual precipitation under the RCP8.5 scenario decreases from 2050 onwards, reaching a $-38 \pm 11\%$ change as a decadal average in 2090–2099. In line with previous studies⁶⁰, a slight decrease in precipitation is projected under the RCP2.6 scenario during the period 2030-2050, followed by a moderate increase by the end of the century. Precipitation deficits during the Chilean megadrought are outside the standard deviation of the selected scenarios for 2000-2019, demonstrating the severity of this event. We note that the reference period (2000-2009) was more humid than the full period used for bias-correcting the GCMs (1990-2019), and both RCP scenarios show negative precipitation anomalies during the reference period (Methods). The projected warming also yields changes in the phase of precipitation over glaciers, with the annual ratio of liquid to total precipitation increasing from 6% to $16 \pm 3\%$ (30 ± 3%) under RCP2.6 (RCP8.5) in 2090–2099 (Supplementary Fig. 13).

The projected warming will have a large impact on glacier volume and mass balance (Fig. 2c-d). Results indicate future reductions in glacier volume of $55 \pm 6\%$ (RCP2.6) and $78 \pm 4\%$ (RCP8.5) and cumulative glacier mass balances of -42 ± 4 m w.e. (RCP2.6) and -58 ± 3 m w.e. (RCP8.5) by the end of the century. We do not project the disappearance of any selected glacier under the RCP2.6 scenario, but we estimate that 15 to 44 of the glaciers included in this study will disappear (i.e., will have more than 99% of volume loss) under the RCP8.5 scenario. Debris-covered glaciers and glaciers north of 34°S will retain more volume than debris-free glaciers and glaciers to the south, respectively (Supplementary Figs. 14-15). The RCP8.5 scenario indicates an annual glacier runoff 11% higher than the reference period for the decade 2036-2046 (i.e. a peak water phase for glacier runoff), followed by a steady decrease until 2100 (Fig. 2e). The RCP2.6 scenario also indicates a phase of peak water for glacier runoff between 2021 and 2031 (6% increase higher than the reference period), followed by a decline and a partial recovery in 2080-2100. This is likely driven by the moderate precipitation increase prescribed under this scenario (Fig. 2b). As a decadal average in 2090-2099, annual glacier runoff changes will be $-7 \pm 2\%$ and $-20 \pm 11\%$ under the RCP2.6 and RCP8.5 scenarios, respectively. The decrease of glacier runoff is projected to be more pronounced during summer, with changes of $-41 \pm 3\%$ (RCP2.6) and $-63 \pm 7\%$ (RCP8.5) in 2090-2099. This is consistent with results from a previous study that included catchments of the Southern Andes in global analyses41.

The role of glaciers during future megadroughts

Here we compare the glacier response to megadroughts projected for the end of the century against the observed glacier response during the Chilean megadrought (sub-period 2010-2019), using the reference period (2000–2009) as a base line (Fig. 3 and Table 1). Given the projected glacier mass loss, glaciers will not be able to compensate the decline in precipitation during future megadroughts in the same way as they have done during the current megadrought. End-of-century megadroughts show mean annual precipitation deficits of $21 \pm 1\%$ (average and standard deviation over GCMs) under RCP2.6 and $39 \pm 10\%$ under RCP 8.5 (Fig. 3a). These changes are similar in magnitude to that of the Chilean megadrought (36% deficit). Moreover, the changes are similar or larger than the precipitation reductions

Table 1 | Summary of changes during the Chilean megadrought (hydrological years 2010-2019) and projected megadroughts under scenarios RCP2.6 and RCP8.5

		Annual			Summer	Annual		
		Total Precipitation mm average across glaciers	Mean air temperature °C	Glacier runoff total volume m³10° sum across glaciers	Glacier runoff total volume m³10 ⁶ sum across glaciers	Ice mett total volume m³10 ⁶ sum across glaciers	Snowmelt total volume m³·10° sum across glaciers	Rainfall total volume $m^3 10^6$ sum across glaciers
Reference period (2000–2009)		1849	-2.3	2153	1249	384	1537	231
Change		, wm %	ي ي	m³·10 ⁶ %	m³·10 ⁶ %	m³·10 ⁶ %	m³10 ⁶ %	m³·10 ⁶ %
Chilean megadrought	2010-2019	_662 _35.8	+0.2	_30.3 1.4	-3.4 -0.3	+453.7 +118.0	_491.4 _32.0	+7.4 +3.2
	Driest year (2019)	1220 66.0	+0.9	+542.2 +25.2	+264.4 +21.2	+1499.7 +390.1	_920.2 _59.9	_37.2 _16.1
RCP2.6 megadroughts	10-year	-390 ± 14 -27.7 ± 7	$+1.4 \pm 0.2$	-208.0 ± 94.8 -9.7 ± 4.4	-432.4 ± 32.2 -34.6 ± 2.6	-11.9 ± 55.5 -3.1 ± 14.4	-366.0 ± 28.8 -23.8 ± 1.9	$+170.0 \pm 50.5$ $+73.5 \pm 21.8$
	Driest year	-980 ± 122 -53.0 ± 7	$+1.2 \pm 0.5$	-583.1 ± 81.9 -27.1 ± 3.8	-441.1 ± 101.3 -35.3 ± 8.1	$+221.1 \pm 178.0$ $+57.5 \pm 46.3$	-856.1 ± 134.4 -55.7 ± 8.7	$+51.9 \pm 35.4$ $+22.4 \pm 15.3$
RCP8.5 megadroughts	10-year	-720 ± 190 -38.9 ± 10	$+4.5 \pm 0.4$	-418.9 ± 237.4 -19.5 ± 11.0	-593.8 ± 75.2 -47.6 ± 6.0	$+141.5 \pm 40.2$ $+36.8 \pm 10.5$	-814.2 ± 140.2 -53.0 ± 9.1	$+253.8 \pm 89.8 + 109.7 \pm 38.8$
	Driest year	-1119 ± 197 -60.5 ± 11	$+4.4 \pm 0.3$	-743.9 ± 244.6 -34.6 ± 11.4	-523.9 ± 146.3 -42.0 ± 11.7	$+224.7 \pm 95.5 +58.5 \pm 24.8$	-1094.9 ± 111.9 -71.2 ± 7.3	$+126.3 \pm 71.9$ $+54.6 \pm 31.1$

Italics are used for percentage variations. The confidence intervals for the variables in the RCP scenarios show the standard deviation between GCMs.

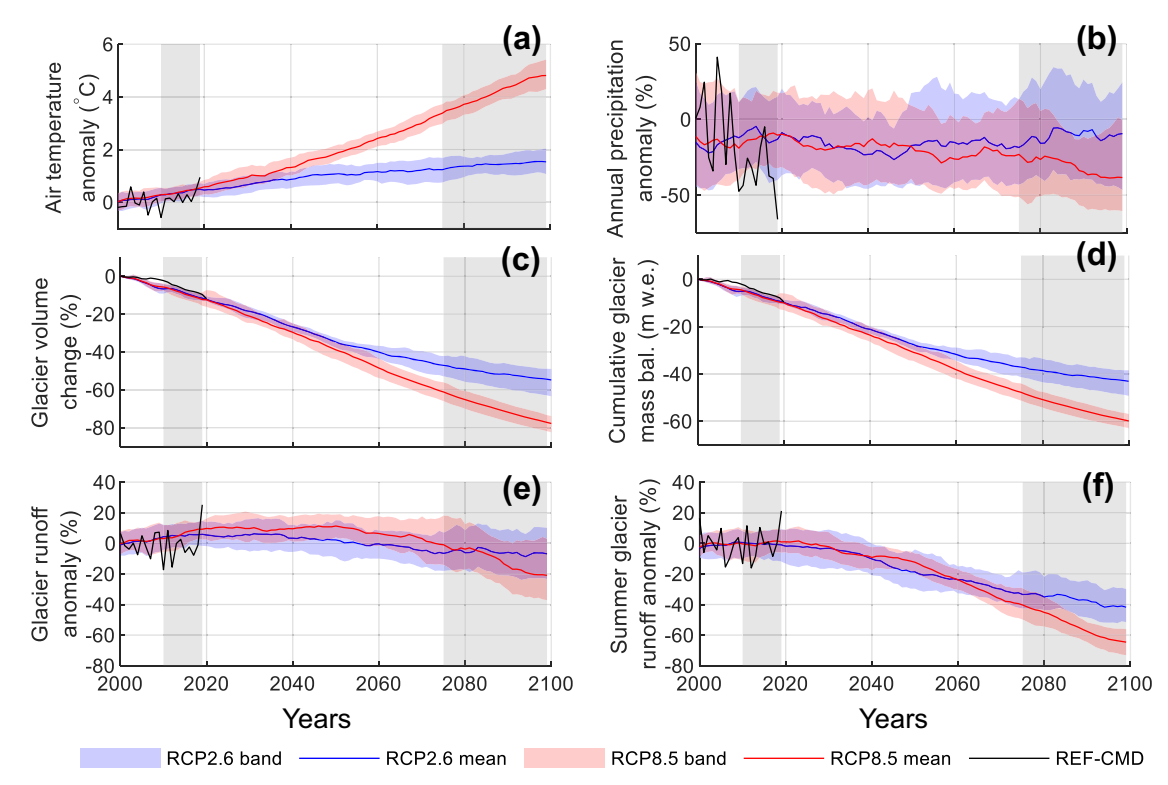


Fig. 2 | Climate and glacier changes under the RCP2.6 and RCP8.5 scenarios for the 100 selected glaciers. a anomaly of annual mean air temperature, b anomaly of annual total precipitation, c changes in total glacier volume, d cumulative glacier mass balance, e anomaly of total glacier runoff, and f anomaly of summer glacier runoff. Anomalies of air temperature, precipitation and glacier runoff are relative to the reference period (2000–2009, REF). Changes in glacier and mass balance are relative to their initial values (year 2000). The continuous lines and the shaded areas in red and blue represent

the averages and the ranges provided by the sample of GCMs under each scenario, respectively. Black lines represent the model results for the reference (REF) and the Chilean megadrought (CMD) periods (2000–2019). The grey shaded areas indicate the Chilean megadrought (2010-2019) and the future period in which we search for 10-year megadroughts (see next section). In Supplementary Fig. 16 we present the same changes presented here using absolute values. A summary of the average values for the 2090-2099 decade is presented in Supplementary Table 1.

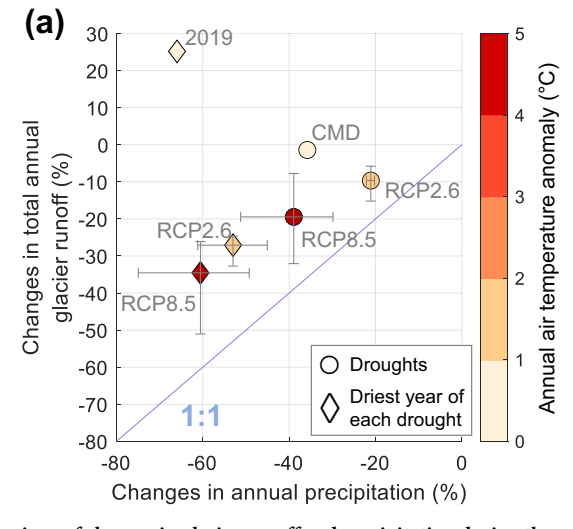
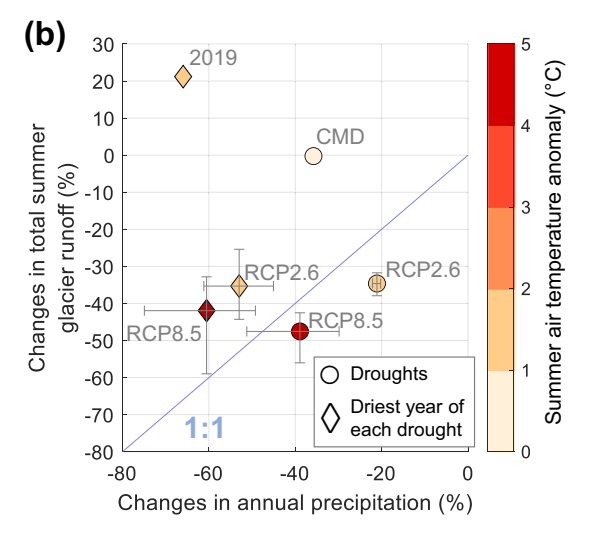


Fig. 3 | Comparison of changes in glacier runoff and precipitation during the current and projected megadroughts. Percent changes in total glacier runoff (y-axis) and annual precipitation (x-axis) during the Chilean megadrought (CMD) and its driest year (2019), as well as for the projected megadroughts and their driest years. Megadroughts and their driest year are represented by circles and diamonds,



respectively. Changes in total glacier runoff refer to (a) annual and (b) summer (JFM) values, respectively. The circles represent the average between GCMs and error bars represent their total range. The colour of each marker indicates the air temperature anomaly averaged over GCMs for each corresponding period. All changes are compared to the 2000–2009 period.

calculated by Chen et al.⁶¹ for the ten most severe megadroughts globally since 1980, which are in general above a 20% deficit. In contrast to the almost unchanged glacier runoff during the Chilean megadrought (-1% variation), glacier runoff significantly diminishes by $10\pm4\%$ (20 $\pm11\%$) for the RCP2.6 (RCP8.5) scenario (significance at a 5% level). Ice melt decreases by

 $4\pm14\%$ under RCP2.6 and it increases by $37\pm11\%$ under RCP8.5, which is far from the 118% increase estimated for the Chilean megadrought, when more ice volume was available for melting (Table 1). The results show that the driest year of the Chilean megadrought (2019) was drier (precipitation deficit of 66%) than 60% of the driest years of each end-of-century

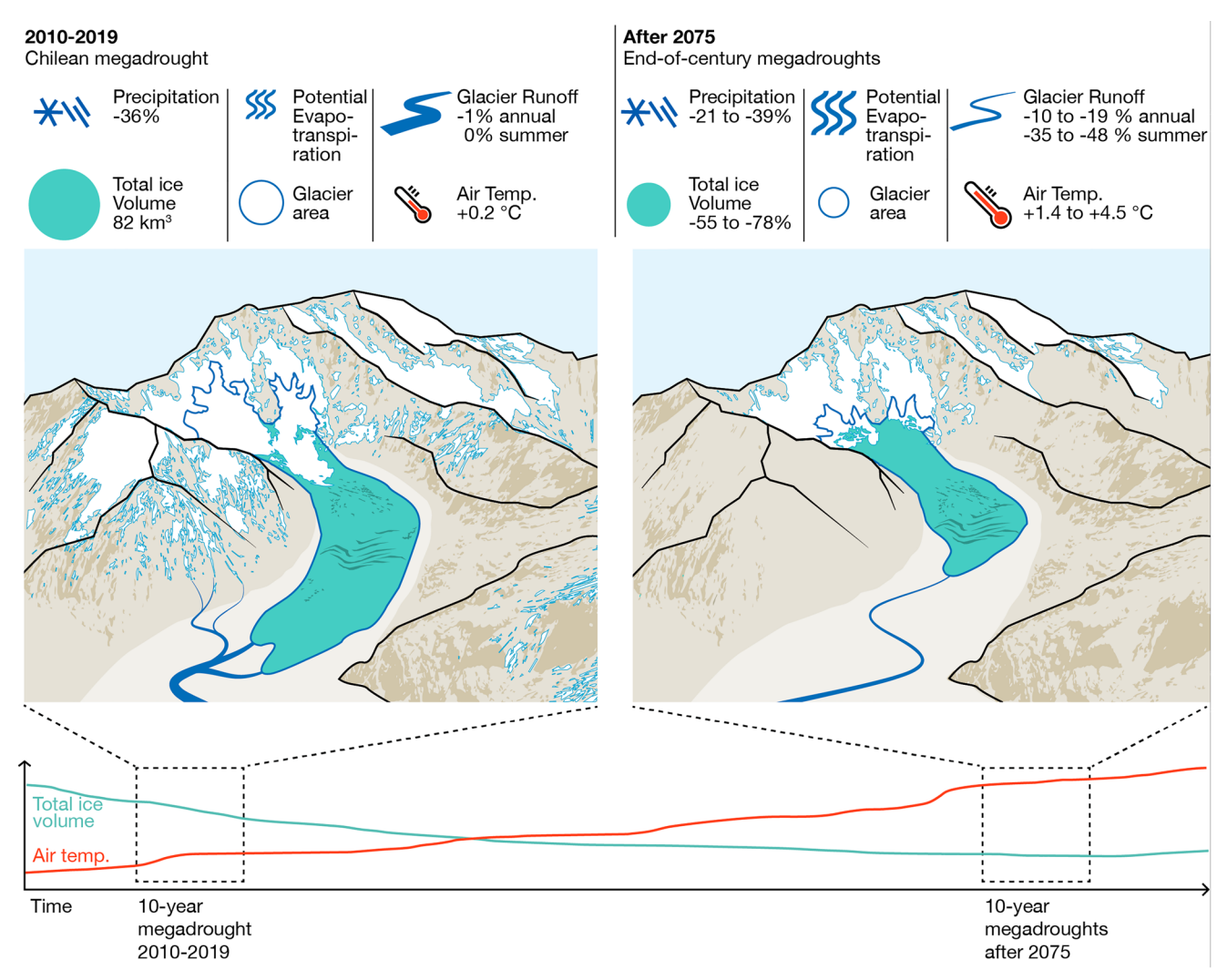


Fig. 4 | Hydrological response of glaciers to the current and projected megadroughts. Summary of changes in precipitation, air temperature, glacier volume and glacier runoff during the Chilean megadrought and the projected 10-year duration end-of-century (after 2075) megadroughts under RCP scenarios 2.6 and 8.5.

Changes in precipitation, air temperature and glacier runoff are relative to the reference period (2000-2009, REF). Changes in total ice volume are relative to their initial values (year 2000). Given the projected increases in air temperature, we also anticipate an increase of potential evapotranspiration in downstream areas.

megadrought (estimated deficits are $53 \pm 7\%$ and $61 \pm 11\%$ for the selected scenarios, Fig. 3a and Supplementary Fig. 10). However, glacier runoff during these projected driest years is much lower than that in 2019. In fact, while glacier runoff increased by 25% during 2019, buffering the dramatic water scarcity, it is projected to decrease by $27 \pm 4\%$ and $35 \pm 11\%$ during the future megadroughts under the RCP2.6 and RCP 8.5 scenarios, respectively. This indicates that, by the end of the century, glaciers will have exhausted their water provision capacity. Summer glacier runoff is also projected to be lower during future megadroughts than during the Chilean megadrought, varying between $-35 \pm 3\%$ for RCP2.6 and $-48 \pm 6\%$ for RCP8.5. This suggests very strong glacier runoff deficits during the warmest season. In contrast to the Chilean megadrought, which shows a relatively low temperature anomaly, end-of-century megadroughts are projected to occur under higher temperatures ($+1.4 \pm 0.2$ °C and $+4.5 \pm 0.4$ °C), which can also increase melt rates depending on the availability of snow and ice. In absolute terms, the projected decrease in glacier runoff varies between 208 and 419 million m³ a⁻¹, depending on the emission scenario (1-2 times the capacity of El Yeso Reservoir). We expect that glacierised catchments will become less resilient to droughts, increasing their dependence on annual precipitation for runoff. This trend is evident in the values under global climate projections, as they move closer to the 1:1 precipitation-runoff line (Fig. 3). We present our main findings in a graph that summarizes the

observed and projected changes in precipitation, air temperature, glacier volume and glacier runoff during the Chilean megadrought and the end-of-century projected megadroughts (Fig. 4).

Discussion

We assessed the hydrological response of the 100 largest glaciers in the Southern Andes between 30 and 40°S during the Chilean megadrought, globally one of the most severe, intense, persistent and extensive droughts in recent decades. Additionally, we simulated the future evolution of the selected glaciers and their role during future megadroughts projected to occur by the end of the 21st century, using climate projections under RCP2.5 and RCP8.5 scenarios. The Chilean megadrought caused a mean annual precipitation deficit of $36 \pm 12\%$ across glaciers, but total glacier runoff remained virtually unchanged (decrease of 1%) due to a 10% loss in total glacier volume that resulted in a 118% increase in total ice melt. Our results unravel the relative contributions of snowmelt, ice melt and rainfall to runoff in glacierized basins during the megadrought, expanding on previous studies that estimated total glacier runoff based on glacier imbalance or total runoff (See Supplementary Table 2 for a detailed comparison 30,38,42,62). In terms of mechanisms, our simulations show that the observed glacier imbalance during the Chilean megadrought was largely driven by the precipitation deficit and less by the slight increase of air temperature compared

to the reference period (Fig. 1c). This can be explained by the high sensitivity that glaciers in the semi-arid Andes have towards precipitation deficits and albedo decrease, in turn due to the strong solar radiation that characterizes the area 63,64 . As shown by our simulations (Supplementary Figs. 17 and 18) precipitation deficits led to a strong decrease in glacier albedo and thus to largely enhanced glacier melt. The high sensitivity of the study glaciers towards albedo changes highlights the importance of explicitly accounting, at high spatial and temporal resolutions, for the decay in surface albedo due to snow aging, as well as the differences between snow and bare-ice albedo, when modelling glacier evolution, particularly in regions with a strong solar irradiance and interannual variability of precipitation. A combined effect of low precipitation and high air temperature occurred during 2019, which was the driest and warmest year in our study period. This resulted in a highly negative glacier mass balance ($-1.8\pm1.0~\mathrm{m}$ w.e. a^{-1}), notably more negative than the megadrought average ($-0.8\pm0.5~\mathrm{m}$ w.e. a^{-1}).

Our results project a decline in the water discharge from glacierized basins during future megadroughts in the Southern Andes, indicating that glaciers in this region will no longer be able to mitigate the impact of future droughts to the same extent as they did during the current megadrought. Although future projections of precipitation and runoff are subject to considerable uncertainty and may lie within the range of natural variability, it has been suggested that the substantial reduction in ice volume driven by projected temperature increases allows for a more confident estimation of declining water discharge in mountain catchments⁶⁵. Indeed, our results show that in contrast to the relatively small changes in glacier runoff observed during 2010-2019, glacier runoff is projected to decrease substantially during end-of-century megadroughts compared to the reference period (2000-2009): by $10 \pm 4\%$ under RCP2.6 and by $20 \pm 11\%$ under RCP8.5 on an annual basis, and by $35 \pm 3\%$ and $48 \pm 6\%$ during summer. Crucially, these future megadroughts will occur under substantially warmer conditions than the current megadrought, accelerating melt rates and increasing potential evapotranspiration of downstream areas. We estimate that the projected increase in air temperature over glaciers in the Southern Andes will result in massive glacier volume loss with estimated changes of $-55 \pm 6\%$ (RCP2.6) and $-78 \pm 4\%$ (RCP8.5) relative to year 2000. The loss of glacier ice during future megadroughts will further impact glacier runoff by the last decade of the century, with even greater decreases expected depending on the climate scenario. We project that summer glacier runoff will decrease by 41 \pm 3% (RCP2.6) and 63 \pm 7% (RCP8.5) during the 2090-2099 decade. This reduction in runoff compensation by glaciers derives from the strong glacial retreat projected for the 21st century. Although our study includes several key processes driving glacier mass balance and runoff, our projections should be interpreted considering key limitations that remain in our modelling approach, such as the static representation of debris cover and uncertainties in future climate forcings and glacier dynamics (see Supplementary Note 2 for more details).

Our findings provide a quantification of glaciers role in buffering megadroughts over the evolving trajectories of glacier decline and increased temperature of the 21st century. They demonstrate the complexity and nonlinear dynamics of the cryosphere response, and show how, at the end of the century, future megadroughts could impact mountain systems that have lost their capacity to compensate for precipitation deficits. This new understanding and the framework developed here will enable the anticipation of future water scarcity scenarios, especially in mountain regions facing glacier retreat and increased drought frequency and severity.

Methods

Glacier data

We extract the glacier outlines of the 100 largest glaciers in the Southern Andes between 30°S and 40°S (Fig. 1a) from the Randolph Glacier Inventory version 6.0 (RGIv6.0)³³. We find that five large glacier polygons in the RGIv6.0 could be divided into two or more individual glaciers, according to a more detailed national inventory from Chile⁶⁶, resulting in a total of 113 glacier polygons that are here treated as independent modelling units (Fig. 1b). We obtain surface topography from the Shuttle Radar Topography

Mission (SRTM)⁶⁷ digital elevation model (DEM), distributed ice thickness for the year 2000 from Farinotti et al.68, and distributed supraglacial debris thickness from Rounce et al.⁶⁹. These datasets are bilinearly resampled to a 100×100 m regular grid. The selected glaciers comprise a total of 82.0 km³ of ice volume distributed over 1044 km², representing 65.8% and 49.2% of the total glacier volume and area of the Southern Andes between 30 and 40°S, respectively. 320 km² of this area (i.e. 31% of the total) is covered by debris. The elevation of the selected glaciers ranges between 1580 and 6709 m a.s.l., with a decreasing trend towards south (Supplementary Fig. 1a). Most of the glacier areas range between 1 and 40 km², but the Tupungato Sur/Tunuvan Glacier reaches up to 69.3 km² (Supplementary Fig. 1b). Although Universidad Glacier is the largest glacier of the study region in the RGIv6.0 (111 km²), this is one of the glaciers that we divided into several modelling units. Debris coverage varies from 0 to 90% of the total glacier area (Supplementary Fig. 1c). The decision of focusing on only the 100 largest glaciers was partly made due to the computational restraints of running a 100 m resolution hydrological model at a 3-hour timestep. The remaining glaciers in our study region are smaller than 1.1 km². In line with the findings of Huss and Fischer⁷⁰, we believe that their integrated response to projected changes is likely to be a mixed one, modulated by a rapid, sensitive response of steep mountain glaciers with a large elevation range (i.e. Tapado Glacier, Robson et al. 71) and a slow, insensitive response of highelevation glacierets and low-elevation glaciers covered by a thick debris layer.

We use glacier surface elevation changes from Hugonnet et al.44 and surface albedo from Moderate Resolution Imaging Spectroradiometer (MODIS)⁵⁰ products as reference (i.e., observational) datasets to calibrate and evaluate TOPKAPI-ETH for the period 2000-2019 (see next sections). Glacier surface elevation changes are converted to mass changes using a glacier density of 850 kg m⁻³⁷². Spatially distributed surface albedo is calculated at a 500 m horizontal resolution for the period 2000-2018 from the average of MOD10A1 (Terra) and MYD10A1 (Aqua) snow products provided by MODIS. Daily and monthly time series of glacier-wide surface albedo are calculated for each glacier using only the 500 m grid cells completely contained within the glacier boundaries. Grid cells without satellite information are filled with data from their neighbours or from other time steps, based on the methodology described by Gafurov and Bárdossy⁷³. From the daily time series, we identify the date with the minimum glacierwide albedo and extract the corresponding albedo map to be used as a base albedo map in TOPKAPI-ETH when the seasonal snow cover disappears.

Meteorological data

Glacier model simulations are forced using precipitation, air temperature and cloud cover transmissivity of solar radiation at a 3-hour time step. The first two variables are derived from the CR2Met v2.0 gridded meteorological product (CR2Met v2.0)⁵¹, which contains daily maps of precipitation and air temperature extremes at $0.05^{\circ} \times 0.05^{\circ}$ resolution over the period 1979-2020. The CR2Met v2.0 products were generated by the Centre for Climate and Resilience Research (CR2) for Chile and the eastern slope of the Andes Cordillera. The CR2Met v2.0 daily total precipitation product was generated through a statistical post-processing approach, based on regression models between in-situ quality-controlled daily precipitation and moisture fluxes from the ERA5 reanalysis⁵², as well as topographic descriptors as predictors⁷⁴. CR2Met v2.0 also includes maps of daily extreme air temperatures that were obtained using near-surface temperature from ERA5 and land surface temperature (LST) from the Moderate Resolution Imaging Spectroradiometer (MODIS), by means of multiple linear regression models using local observations as predictands, and LST as one of the explanatory variables. We average CR2Met maps of daily extremes to obtain daily mean air temperature maps.

We disaggregate the maps of daily precipitation amounts and daily mean air temperature to a 3-hour time step following the sub-daily distribution of the same variables from ERA5 (interpolated to the CR2Met grid). For each glacier, we calculate 3-hour air temperature lapse rates by fitting a linear regression model between the temperature and the elevation

of the eight CR2Met grid cells that surround the cell corresponding to the glacier centroid. Using the daily average of the 3 h lapse rates, we transfer the 3-hour air temperatures from the linearly interpolated CR2Met grid to the centroid of each glacier adjusting by the elevation difference. Daily average air temperature lapse rates are also used in TOPKAPI-ETH to distribute air temperature over the elevation profile of each glacier (see next section). Time series of cloud cover transmissivity are derived directly from the ERA5 atmospheric reanalysis as the fraction between the total sky direct solar radiation at the surface and the clear sky direct solar radiation at the surface variables. Precipitation and cloud cover transmissivity are linearly interpolated to the centroid of each glacier without further correction.

For climate and hydrological future projections, we use outputs from four CMIP5 GCMs (CCSM4, CSIRO-MK3-6-0, IPSL-CM5A-LR and MIROC-ESMI), which are selected based on two attributes: (1) their ability to represent observed climate patterns in continental Chile at regional and large-scale level, and (2) the spread these models provide for projected changes in annual precipitation and temperature, which is similar in magnitude to that obtained using the full CMIP5 multi-model ensemble⁷⁴. Given the high temporal and horizontal resolution of our glacier simulations (see next section), we decided not to include further GCMs. The selected emission scenarios are representative of moderate (RCP2.6) and high (RCP8.5) Greenhouse gas (GHG) emissions⁷⁵. We use 1990/04/01-2020/ 03/31 (i.e., 30 water years) as the reference period for downscaling. The steps of downscaling and bias correction are essential to move from the coarse resolution outputs of the GCMs to the fine scale of the glacio-hydrological simulations. The horizontal resolution of the GCMs is between 1° and 4° and their time step is daily (see details in Supplementary Table 3). The downscaling procedure consists of a bilinear interpolation to the glacier centroid and a bias correction method performed following the Multivariate Bias Correction for n-dimensions (MBCn) approach proposed by Cannon⁵⁴ and recommended for snowmelt-driven high-elevation catchments⁵⁵. This downscaling method explicitly considers the covariation between the probability density functions of different variables, in our case, daily precipitation, daily average temperature and maximum and minimum air temperature. Although we also tested the original Quantile Delta Mapping (QDM) method and other multivariate QDM strategies⁷⁶, MBCn yielded the best results. Finally, we disaggregated each of the daily meteorological values from the GCMs using sub-daily distributions extracted from days in the corresponding months of the reference period with the most similar precipitation and extreme temperatures. To do so, we compute the Euclidean distance between the three variables retrieved for the target day in the GCMs data and the candidates of the reference period and keep the one day that minimizes this distance. Results of the downscaling procedure for all the modelling units are presented in the Supplementary Figs. 8 and 9.

TOPKAPI-ETH

TOPKAPI-ETH is a physically oriented, spatially distributed hydrological model that simulates the mass balance, evolution, and runoff contribution of glaciers, along with snow accumulation, snow-ice transition, glacier dynamics, snow melt, ice melt and ice melt under debris⁷⁷. Due to its physics-oriented configuration, TOPKAPI-ETH can be applied to other mountain catchments in the world without substantial reconfiguration (only recalibration of parameters). For example, it has been applied to several catchments in the semi-arid Andes^{37,45} and other mountainous regions around the world^{77–79}. The model includes a parametrization of glacier dynamics, which updates glacier elevation and area as a function of surface mass balance (Δ h-parameterization)⁴⁸. This module is essential to accurately simulate glacio-hydrological responses in decadal-scale simulations.

Following the strategy applied by Ayala et al.³⁷ in the Maipo River basin (central Chile), TOPKAPI-ETH is applied for each glacier individually. The domain of each model is defined as the glacier area, and we adopt a 100 m horizontal resolution and a time step of 3 h for model simulations, in line with the available glacier and climate data (see previous sections). While precipitation and cloud cover transmissivity are assumed to be spatially

uniform over each glacier, air temperature is distributed over the 100 m grid from the centroid of each glacier using the lapse rates derived in the previous section. The models are run from 25 May 1999, just before a precipitation event that affected most glaciers in the study region. We selected this starting date as it allows the model to have a spin-up period without excessively altering the initial ice thicknesses, which were extracted from Farinotti et al. 68 and correspond to the beginning of year 2000. We use the same set of model parameters as in Ayala et al.³⁷, except seven parameters that are calibrated independently for each modelling unit over the period 2000-2015, using 2015-2019 as an evaluation period. The calibrated parameters adjust precipitation and air temperature from the scale of CR2Met v2.0 to the glacier local scale (2 parameters), the albedo decay rate (1 parameter), melt factors for snow and debris-free ice (2 parameters) and melt factors for debriscovered ice (2 parameters). We apply an optimization algorithm to simultaneously minimize the differences between (a) observed and simulated glacier mass balance and (b) monthly time series of glacier-wide surface albedo from MODIS products. We seek to maximize a meta-objective function (F) that combines observed glacier-wide monthly average albedo and geodetic mass balance as target objective criteria:

$$F = 1$$

$$-\sqrt{0.7 * (MBE - 1)^2 + 0.3 * (0.3 * (r_{albedo} - 1)^2 + 0.7 * (e_{albedo} - 1)^2)}$$
(1)

Where r_{albedo} is the Pearson correlation coefficient between observed and simulated values. Additionally:

$$MBE = 1 - \left| \frac{\Delta M_{Sim2000 - 2015} - \Delta M_{Obs2000 - 2015}}{\Delta M_{Obs2000 - 2015}} \right|$$
 (2)

and

$$e_{albedo} = 1 - \sqrt{\frac{1}{T} \sum_{t=1}^{T} \left(\frac{albedo_{sim} - albedo_{MODIS}}{albedo_{MODIS}} \right)^2}$$
(3)

The terms $\Delta M_{Sim2000-2015}$ and $\Delta M_{Obs2000-2015}$ correspond to the mass balance between 2000 and 2015 calculated from the TOPKAPI-ETH simulations and the geodetic mass balance from Hugonnet et al. 44 , respectively.

To maximize F, we use the Shuffled Complex Evolution (SCE-UA⁸⁰) global optimization algorithm. The parameter sets that produce the best results are used as a basis for producing new parameter sets, and those yielding poor model performances are gradually discarded. We limit the precipitation factors within the range 0.5 and 2.5, and the temperature offsets within -3 and 3 °C. These ranges are similar to those used in other glacier modelling studies^{62,81,82}. Additionally, we impose the restriction that the melt factors for debris-covered ice (SRFd and TFd) must be lower than those for snow and debris-free ice (SRF and TF). For the final analysis, we discarded the results of four glaciers, for which the MODIS albedo was not available (considering the scarcity of neighbouring pixels with information), and the bias of the (calibrated) simulated geodetic mass balance was off by more than 1 m w.e. a⁻¹. A summary of results from the calibration and validation procedures is shown in the Supplementary Figs. 2-7. The parameter values obtained in the optimisation procedure are well distributed over the range chosen for each parameter. In line with previous findings on the uncertainty and sensitivity analysis of TOPKAPI-ETH applied to Andean basins, during the calibration process, we verified that the objective function is most sensitive to variations of the precipitation factor and, in the case of debris-covered glaciers, to the melt factors for ice melt under debris. For a more detailed view on the uncertainty and sensitivity of TOPKAPI-ETH parameters, we refer the reader to these previous studies^{36,77,83}. In the Supplementary Note 2 we include a more detailed list of the limitations in our study associated with parametric uncertainty and other sources.

Future megadroughts

As we ignore the specific hydrologic characteristics under which future droughts will develop, we work directly with meteorological droughts. We define end-of-century megadroughts as the driest 10-year periods in the period 2075-2100. To this end, we calculate a 10-year moving average of the statistically downscaled precipitation (average across glaciers) for each GCM and scenario and identify the lowest value and period of occurrence. Our choice of period length is made to approximate the duration of the Chilean megadrought.

Data availability

The results of TOPKAPI-ETH simulations and processed files for this article are available at https://doi.org/10.5281/zenodo.17105125. The annual time series of the main glaciological variables are also available in the same link.

Code availability

The files necessary to run TOPKAPI-ETH at each of the study glaciers and the scripts that processed the final datasets are available at https://doi.org/10.5281/zenodo.17105125.

Received: 30 November 2024; Accepted: 29 September 2025; Published online: 18 November 2025

References

- Kannenberg, S. A. et al. Linking drought legacy effects across scales: from leaves to tree rings to ecosystems. *Glob. Chang. Biol.* 25, 2978–2992 (2019).
- Yang, Y. et al. Contrasting responses of water use efficiency to drought across global terrestrial ecosystems. Sci. Rep. 6, 1–8 (2016).
- Mullin, M. The effects of drinking water service fragmentation on drought-related water security. Science 368, 274–277 (2020).
- Rakovec, O. et al. The 2018–2020 multi-year drought sets a new benchmark in Europe. Earth's Future 10 at https://doi.org/10.1029/ 2021EF002394 (2022).
- Stahl, K. et al. Impacts of European drought events: Insights from an international database of text-based reports. *Nat. Hazards Earth Syst. Sci.* 16, 801–819 (2016).
- Cook, B. I. et al. Megadroughts in the Common Era and the Anthropocene. Nat. Rev. Earth Environ. 3, 741–757 (2022).
- Williams, A. P. et al. Large contribution from anthropogenic warming to an emerging North American megadrought. *Science* 370, 314–318 (2020).
- Howitt, R., Medellín-azuara, J. & Macewan, D. Economic Analysis of the 2014 Drought for California Agriculture. Cent. Watershed Sci. Univ. California, Davis, Calif. 20p (2014).
- Naumann, G., Cammalleri, C., Mentaschi, L. & Feyen, L. Increased economic drought impacts in Europe with anthropogenic warming. *Nat. Clim. Chang.* 11, 485–491 (2021).
- Su, B. et al. Drought losses in China might double between the 1.5 °C and 2.0 °C warming. Proc. Natl. Acad. Sci. USA 115, 10600–10605 (2018).
- 11. Satoh, Y. et al. The timing of unprecedented hydrological drought under climate change. *Nat. Commun.* **13**, 3287 (2022).
- Seneviratne, S. I. et al. Weather and Climate Extreme Events in a Changing Climate. in Climate Change 2021: The Physical Science Basis. Contribution of Working Group I to the Sixth Assessment Report of the Intergovernmental Panel on Climate Change (eds. Masson-Delmotte, V. P. Z., A. Pirani, S. L. Connors, C. Péan, S. Berger, N. Caud, Y. Chen, L. Goldfarb, M. I. Gomis, M. Huang, K. Leitzell, E. L. & J.B.R. Matthews, T. K. Maycock, T. Waterfield, O. Yelekçi, R. Yu, B. Z.) 1513–1766 (Cambridge University Press, 2021).
- Van Loon, A. F. et al. Drought in the Anthropocene. Nat. Geosci. 9, 89–91 (2016).
- Garreaud, R. D. et al. The 2010-2015 megadrought in central Chile: Impacts on regional hydroclimate and vegetation. *Hydrol. Earth Syst. Sci.* 21, 6307–6327 (2017).

- Masiokas, M. H. et al. A Review of the Current State and Recent Changes of the Andean Cryosphere. Front. Earth Sci. 8, 1–27 (2020).
- Álamos, N., Alvarez-Garretón, C., Muñoz, A. & González-Reyes, Á The influence of human activities on streamflow reductions during the megadrought in central Chile. *Hydrol. Earth Syst. Sci.* 28, 2483–2503 (2024).
- Observatory of Economic Complexity. Chile. https://oec.world/en/ profile/country/chl (2025).
- Observatory of Economic Complexity. Argentina. https://oec.world/ en/profile/country/arg (2025).
- Garreaud, R. D. et al. The Central Chile Mega Drought (2010–2018): A climate dynamics perspective. *Int. J. Climatol.* 40, 421–439 (2020).
- González-Reyes, Á. et al. Recent multispecies tree-growth decline reveals a severe aridity change in Mediterranean Chile. *Environ. Res. Lett.* 19 (2024).
- Morales, M. S. et al. Six hundred years of South American tree rings reveal an increase in severe hydroclimatic events since mid-20th century. *Proc. Natl. Acad. Sci. USA* 117, 16816–16823 (2020).
- 22. European Commission, J. R. C. (JRC). Drought events based on SPEI 12 version 1.0. at http://data.europa.eu/89h/154f7ef5-17da-481f-b6e6-2933db1c7af3 (2017).
- Spinoni, J. et al. A new global database of meteorological drought events from 1951 to 2016. J. Hydrol. Reg. Stud. 22, 100593 (2019).
- Boisier, J. P., Rondanelli, R., Garreaud, R. D. & Muñoz, F. Anthropogenic and natural contributions to the Southeast Pacific precipitation decline and recent megadrought in central Chile. *Geophys. Res. Lett.* 43, 413–421 (2016).
- Masiokas, M. H. et al. Streamflow variations across the Andes (18°–55°S) during the instrumental era. Sci. Rep. 9, 1–13 (2019).
- Fuentealba, M., Bahamóndez, C., Sarricolea, P., Meseguer-Ruiz, O. & Latorre, C. The 2010–2020 'megadrought' drives reduction in lake surface area in the Andes of central Chile (32°-36°S). J. Hydrol. Reg. Stud. 38, (2021).
- Lema, F. et al. Technical note: What does the Standardized Streamflow Index actually reflect? Insights and implications for hydrological drought analysis. *Hydrol. Earth Syst. Sci.* 29, 1981–2002 (2025).
- González, M. E., Gómez-González, S., Lara, A., Garreaud, R. & Díaz-Hormazábal, I. The 2010–2015 Megadrought and its influence on the fire regime in central and south-central Chile. *Ecosphere* 9, https://doi.org/10.1002/ecs2.2300 (2018).
- Vergara, I., Garreaud, R. & Ayala, Á Sharp Increase of Extreme Turbidity Events Due To Deglaciation in the Subtropical Andes. J. Geophys. Res. Earth Surf. 127, 1–15 (2022).
- McCarthy, M. et al. Glacier contributions to river discharge during the current Chilean Megadrought. Earth's. Futur 10, 1–15 (2022).
- 31. Muñoz, A. A. et al. Water crisis in Petorca Basin, Chile: The combined effects of a mega-drought and water management. *Water* **12**, (2020).
- 32. Pritchard, H. D. Asia's shrinking glaciers protect large populations from drought stress. *Nature* **569**, 649–654 (2019).
- 33. RGI Consortium. Randolph Glacier Inventory—A Dataset of Global Glacier Outlines, Version 6. at (2017).
- Masiokas, M. H., Villalba, R., Luckman, B. H., Le Quesne, C. & Aravena, J. C. Snowpack variations in the central Andes of Argentina and Chile, 1951-2005: Large-scale atmospheric influences and implications for water resources in the region. *J. Clim.* 19, 6334–6352 (2006).
- Mernild, S. H., Liston, G. E., Hiemstra, C. & Wilson, R. The Andes Cordillera. Part III: glacier surface mass balance and contribution to sea level rise (1979–2014). *Int. J. Climatol.* 37, 3154–3174 (2017).
- Ragettli, S. & Pellicciotti, F. Calibration of a physically based, spatially distributed hydrological model in a glacierized basin: on the use of knowledge from glaciometeorological processes to constrain model parameters. Water Resour. Res. 48, 1–20 (2012).

- Ayala, Á. et al. Glacier runoff variations since 1955 in the Maipo River basin, in the semiarid Andes of central Chile. *Cryosphere* 14, 2005–2027 (2020).
- Dussaillant, I. et al. Two decades of glacier mass loss along the Andes. Nat. Geosci. 12, 802–808 (2019).
- van Tiel, M. et al. Melting Alpine water towers aggravate downstream low flows: a stress-test storyline approach. Earth's. Futur 11, 1–23 (2023).
- Ultee, L., Coats, S. & Mackay, J. Glacial runoff buffers droughts through the 21st century. Earth Syst. Dyn. 13, 935–959 (2022).
- Huss, M. & Hock, R. Global-scale hydrological response to future glacier mass loss. *Nat. Clim. Chang.* 8, 135–140 (2018).
- Caro, A., Condom, T., Rabatel, A., Aguayo, R. & Champollion, N. Future glacio-hydrological changes in the Andes: a focus on nearfuture projections up to 2050. Sci. Rep. 15, 1–13 (2025).
- 43. Braun, M. H. et al. Constraining glacier elevation and mass changes in South America. *Nat. Clim. Chang.* **9**, 130–136 (2019).
- Hugonnet, R. et al. Accelerated global glacier mass loss in the early twenty-first century. *Nature* 592, 726–731 (2021).
- Ragettli, S., Immerzeel, W. W. & Pellicciotti, F. Contrasting climate change impact on river flows from high-altitude catchments in the Himalayan and Andes Mountains. *Proc. Natl. Acad. Sci. USA* 113, 9222–9227 (2016).
- Davaze, L. et al. Monitoring glacier albedo as a proxy to derive summer and annual surface mass balances from optical remote-sensing data. Cryosphere 12, 271–286 (2018).
- 47. Naegeli, K. & Huss, M. Sensitivity of mountain glacier mass balance to changes in bare-ice albedo. *Ann. Glaciol.* **58**, 119–129 (2017).
- 48. Huss, M., Jouvet, G., Farinotti, D. & Bauder, A. Future high-mountain hydrology: A new parameterization of glacier retreat. *Hydrol. Earth Syst. Sci.* **14**, 815–829 (2010).
- Zekollari, H., Huss, M., Farinotti, D. & Lhermitte, S. Ice-dynamical glacier evolution modeling — a review. Rev. Geophys. 60 at https://doi. org/10.1029/2021RG000754 (2022).
- Hall, D. K., Riggs, G. A., Salomonson, V. V., Digirolamo, N. E. & Bayr, K. J. MODIS snow-cover products. 83, 181–194 (2002).
- Boisier, J. P. CR2MET: A high-resolution precipitation and temperature dataset for the period 1960-2021 in continental Chile. at https://doi.org/10.5281/zenodo.7529682 (2023).
- Hersbach, H. et al. The ERA5 global reanalysis. Q. J. R. Meteorol. Soc. 146, 1999–2049 (2020).
- Taylor, K. E., Stouffer, R. J. & Meehl, G. A. An overview of CMIP5 and the experiment design. *Bull. Am. Meteorol. Soc.* 93, 485–498 (2012).
- Cannon, A. J. Multivariate quantile mapping bias correction: an N-dimensional probability density function transform for climate model simulations of multiple variables. Clim. Dyn. 50, 31–49 (2018).
- 55. Meyer, J. et al. Effects of univariate and multivariate bias correction on hydrological impact projections in alpine catchments. *Hydrol. Earth Syst. Sci.* **23**, 1339–1354 (2019).
- Farías-Barahona, D. et al. Geodetic mass balances and area changes of Echaurren Norte Glacier (Central Andes, Chile) between 1955 and 2015. Remote Sens. 11, (2019).
- Masiokas, M. H. et al. Reconstructing the annual mass balance of the Echaurren Norte glacier (Central Andes, 33.5° S) using local and regional hydroclimatic data. *Cryosph* 10, 927–940 (2016).
- Ahumada, G., Bustos, D. & González, M. Effect of climate change on drinking water supply in Santiago de Chile. Sci. Cold Arid Reg. 5, 27 (2013).
- Alvarez-Garreton, C., Pablo Boisier, J., Garreaud, R., Seibert, J. & Vis, M. Progressive water deficits during multiyear droughts in basins with long hydrological memory in Chile. *Hydrol. Earth Syst. Sci.* 25, 429–446 (2021).
- Chadwick, C., Gironás, J., Vicuña, S. & Meza, F. Estimating the local time of emergence of climatic variables using an unbiased mapping of GCMs: An application in semiarid and mediterranean Chile. *J. Hydrometeorol.* 20, 1635–1647 (2019).

- Chen, L. et al. Global increase in the occurrence and impact of multivear droughts. Science 387, 278–284 (2025).
- Caro, A. et al. Hydrological response of Andean catchments to recent glacier mass loss. *Cryosphere* 18, 2487–2507 (2024).
- Ayala, Á, Pellicciotti, F., MacDonell, S., McPhee, J. & Burlando, P. Patterns of glacier ablation across North-Central Chile: Identifying the limits of empirical melt models under sublimation-favorable conditions. Water Resour. Res. 53, 5601–5625 (2017).
- Pellicciotti, F. et al. A study of the energy balance and melt regime on Juncal Norte Glacier, semi-arid Andes of central Chile, using melt models of different complexity. *Hydrol. Process.* 22, 3980–3997 (2008).
- 65. Fatichi, S., Rimkus, S., Burlando, P. & Bordoy, R. Does internal climate variability overwhelm climate change signals in streamflow? The upper Po and Rhone basin case studies. *Sci. Total Environ.* **493**, 1171–1182 (2014).
- 66. DGA. Inventario Público de Glaciares, Actualización 2022. (2022).
- 67. Farr, T. et al. Shuttle Radar Topography Mission: Mission to map the world. *Rev. Geophys.* **45**, 3–5 (2007).
- 68. Farinotti, D. et al. A consensus estimate for the ice thickness distribution of all glaciers on Earth. *Nat. Geosci.* **12**, 168–173 (2019).
- Rounce, D. R. et al. Distributed global debris thickness estimates reveal debris significantly impacts glacier mass balance. *Geophys. Res. Lett.* 48 (2021).
- 70. Huss, M. & Fischer, M. Sensitivity of very small glaciers in the swiss alps to future climate change. *Front. Earth Sci.* **4**, 1–17 (2016).
- Robson, B. A. et al. Glacier and rock glacier changes since the 1950s in the La Laguna catchment, Chile. Cryosphere 16, 647–665 (2022).
- Huss, M. Density assumptions for converting geodetic glacier volume change to mass change. Cryosph 7, 877–887 (2013).
- Gafurov, A. & Bárdossy, A. Cloud removal methodology from MODIS snow cover product. Hydrol. Earth Syst. Sci. 13, 1361–1373 (2009).
- 74. DGA. Actualización Del Balance Hídrico Nacional, SIT Nº 417, Ministerio de Obras Públicas, Dirección General de Aguas, División de Estudios y Planificación, Santiago, Chile. Realizado Por: Universidad de Chile & Pontificia Universidad Católica de Chile. (2017).
- Cubash, U. et al. Introduction. in Climate Change 2013: The Physical Science Basis. Contribution of Working Group I to the Fifth Assessment Report of the Intergovernmental Panel on Climate Change (eds. Stocker, T. F. et al.) (Cambridge University Press, 2013). https://doi.org/10.1016/B978-0-12-809665-9.15009-8.
- Cannon, A. J., Sobie, S. R. & Murdock, T. Q. Bias correction of GCM precipitation by quantile mapping: How well do methods preserve changes in quantiles and extremes?. J. Clim. 28, 6938–6959 (2015).
- Ragettli, S. et al. Unraveling the hydrology of a Himalayan catchment through integration of high resolution in situ data and remote sensing with an advanced simulation model. *Adv. Water Resour.* 78, 94–111 (2015).
- Fatichi, S., Rimkus, S., Burlando, P., Bordoy, R. & Molnar, P. Highresolution distributed evaluation of climate and anthropogenic changes on the hydrology of an Alpine catchment. *J. Hydrol.* 525, 362–382 (2015).
- Jouberton, A. et al. Warming-induced monsoon precipitation phase change intensifies glacier mass loss in the southeastern Tibetan Plateau. Proc. Natl. Acad. Sci. USA 119, 1–7 (2022).
- Duan, Q., Sorooshian, S. & Gupta, V. Effective and efficient global optimization for conceptual rainfall-runoff models. Water Resour. Res. 28, 1015–1031 (1992).
- 81. Huss, M. & Hock, R. A new model for global glacier change and sealevel rise. *Front. Earth Sci.* **3**, 1–22 (2015).
- Zekollari, H., Huss, M. & Farinotti, D. Modelling the future evolution of glaciers in the European Alps under the EURO-CORDEX RCM ensemble. *Cryosphere* 13, 1125–1146 (2019).
- Ayala, A. et al. Modelling the hydrological response of debris-free and debris-covered glaciers to present climatic conditions in the semiarid Andes of central Chile. *Hydrol. Process.* 30, 4036–4058 (2016).

Acknowledgements

This research was funded in whole or in part by the Austrian Science Fund (FWF), DOI: 10.55776/16891. The project MegaWat has received funding from the Austrian Science Fund (FWF), Swiss National Science Foundation (SNSF), the Centre for the Development of Industrial Technology (CDTI), Dutch Research Council (NWO), National Research Council (CNR) and the European Union's Horizon Europe Programme under the 2022 Joint Transnational Call of the European Partnership Water4all (Grant Agreement n°101060874). Á.A. acknowledges Fondecyt Postdoc No. 3190732, the WSL programme 'Extremes' through the EMERGE project and together with S.M. ANID-CENTROS REGIONALES R20F0008. E.M.C. thanks ANID National Master scholarship year 2020 N°22200599 and the Swiss National Science Foundation Grant 200021_214907. P.A.M. acknowledges support from the Fondecyt project No. 11200142, and ANID/PIA project No AFB230001.

Author contributions

Á.A. and E.M.C. designed the study with conceptual and methodological inputs from D.F., D.F.B., P.A.M., S.M., J.M., X.V. and F.P. E.M.C. performed the TOPKAPI-ETH simulations and Á.A. the analysis of the results. Á.A. and E.M.C. wrote the original draft. F.P., D.F., P.A.M., J.M., S.M. and X.V. contributed to the final editing.

Competing interests

The authors declare no competing interests.

Additional information

Supplementary information The online version contains supplementary material available at https://doi.org/10.1038/s43247-025-02845-6.

Correspondence and requests for materials should be addressed to Álvaro Avala.

Peer review information Communications Earth & Environment thanks the anonymous reviewer(s) for their contribution to the peer review of this work. Primary Handling Editor: Alireza Bahadori. A peer review file is available.

Reprints and permissions information is available at http://www.nature.com/reprints

Publisher's note Springer Nature remains neutral with regard to jurisdictional claims in published maps and institutional affiliations.

Open Access This article is licensed under a Creative Commons Attribution 4.0 International License, which permits use, sharing, adaptation, distribution and reproduction in any medium or format, as long as you give appropriate credit to the original author(s) and the source, provide a link to the Creative Commons licence, and indicate if changes were made. The images or other third party material in this article are included in the article's Creative Commons licence, unless indicated otherwise in a credit line to the material. If material is not included in the article's Creative Commons licence and your intended use is not permitted by statutory regulation or exceeds the permitted use, you will need to obtain permission directly from the copyright holder. To view a copy of this licence, visit http://creativecommons.org/licenses/by/4.0/.

© The Author(s) 2025